MTHE 493 - Final Report
Optimising the Airflow Over the Rear Wing of a Formula SAE Vehicle Using Adjoint Shape Optimisation

Mathew Jennings
Luca Sardellitti
Samuel Schaffel
Siena Thalassinos

April 10, 2022

Queen's University

Faculty of Engineering & Applied Science
Department of Mathematics and Statistics

Executive Summary

Formula Series Racing is a collection of car racing competitions where the goal is to create a vehicle and race the fastest possible time within the constraints for each category. Formula SAE is a category which is designed for university students. Queen's University has a design team called Queen's Formula SAE Team (QFSAE) which competes in this event.

To improve the performance of their vehicle, QFSAE allocates large amounts of resources and time into designing their vehicle to have optimal aerodynamic performance. In the context of Formula Racing, optimal performance is minimizing aerodynamic resistance (drag) while maintaining sufficient downward force on the vehicle to safely turn around the track corners at high speeds. The vehicle's rear wing significantly impacts its overall aerodynamic characteristics. The goal of this project is to work with QFSAE to optimise the shape of their rear wing, while adhering to the Formula SAE rules, and being seamless to introduce into their existing design. A successfully optimised design is one that reduces the coefficient of drag of the wing by 5%, while maintaining at least 95% of the downforce contributed by the wing.

The mathematical model that governs the aerodynamic characteristics being optimised can be reduced to the study of fluid dynamics and the Navier-Stokes equations. The Navier-Stokes equations are a system of differential equations which model the behaviours of fluids. They are used to determine the velocity and pressure of a fluid for a given set of initial conditions. These equations do not generally have analytic solutions, so approximations such as Reynolds-Averaged Navier-Stokes (RANS) and tools such as Computational Fluid Dynamics (CFD) are used to numerically compute approximations of the theoretical solutions.

Optimising the rear wing over all possible shapes is a complex problem, with the amount of parameters scaling with the complexity of the model being analyzed. Solving the optimisation directly with an exhaustive search is not feasible in terms of computation power required to calculate the solutions to fluid dynamic models. An optimisation technique called adjoint optimisation was used to feasibly work toward a solution. This technique defines a cost function and computes its gradient map at each point on the surface of the object. This sensitivity map implies which direction, inward or outward, to change each point on the object to move toward the optimal shape.

The open source CFD called OpenFOAM was used to perform the numerical analysis of the wing. The validity of the OpenFOAM model was tested by analyzing the simple shapes of a sphere and a cube. After obtaining base values within 5% accuracy of their theoretical values, the adjoint optimisation technique implemented by OpenFOAM was applied to these shapes. The resulting modifications reduced the coefficient of drag significantly over two iterations. Applying the same process to the rear wing, the values for coefficient of drag and lift were calculated to be within 2.8% and 2.0%, respectively, of the validation data received from the QFSAE team. Using the results of the adjoint optimisation on the rear wing, a modified model was created which reduced the coefficient of drag by 3.5% while maintaining 98.2% of the downforce. No further improvements to the model were able to be made through adjoint optimisation on the original wing design. An adjoint optimisation was performed on the modified wing, and by confirming that there were no features on the sensitivity map, local optimimality of this design was concluded. This local minimum is a sufficient solution, to maintain within the problem constraints. To obtain a wing design better than this minimum, larger changes would need to be made to the wing which would invalidate the model in terms of implementation feasibility and not adhering to the Formula SAE rule set.

Contents

List of Figures

List of Tables

1 Introduction and Background Information

Formula cars are a pinnacle of automotive engineering and designed for hours until the best car possible is created (under a specific ruleset). At all levels of Formula racing even the smallest margins can make the biggest gains. From Formula 1 (F1) to university level Formula SAE the goal is simple: Driver and team compete to race a set number of laps around a track in the fastest time possible. Shaving off fractions of a second on a lap can be the difference between winning and losing a race. Despite traveling extremely high speeds (F1 vehicles can travel up to 350 km/h on the track [5]), 80% of the race is not spent at the top speed of the car [6]. Indeed, the drivers must slow down when making turns to prevent them from flying off the track. Formula teams increase the speed at which the car can take turns by increasing the downforce felt by the vehicle. This allows the car to stick to the track when turning at high speeds but comes at the cost of greatly increasing the force of drag on the car during the straights. Thus, the key is to find the balance between reducing drag to maximize top speed, and increasing downforce to allow the car to take corners faster.

One solution to keep high levels of downforce on the car is a wing that goes across the rear creating a force towards the ground on the rear wheels. This is common on almost all Formula vehicles and is called the rear wing. The existence of this massive wing creates large amounts of drag on the straights. Some levels of Formula racing including Formula One and Formula Two even have a system that flattens the rear wing on long straights. At the university level Formula SAE, there is no such drag reduction system. Thus, a way to reduce drag on this rear wing is to modify the shape of the wing, optimising the drag to downforce ratio.

For this project, the QFSAE team, a university level Formula SAE team based at Queen's University, was consulted. The existing rear wing on the QFSAE car was modified with this goal of optimising drag versus downforce. The QFSAE team has competed and will continue to compete at several competitions across North America. These competitions are run by SAE International, a standard developing organization for engineering professionals. The competition includes several different tests that are designed to challenge the teams' engineering design process. This is done by assessing their project management, budgeting, communication, and resource management skills while also testing how their car performs in a range of tests from acceleration to a full race. [7]

For additional background information related to the project - Katz provides an in-depth analysis of the aerodynamics of Formula style cars [8].

2 Problem Description

The problem being addressed is to shorten the lap time of the QFSAE vehicle by optimising its drag force at multiple track positions. This will be achieved by reducing the drag force on straightaways caused by the rear wing by 5%. The design will also maintain at least 95% of its downforce on turns to allow the vehicle to go around corners of the track at a high speed without lifting off the ground. When optimising this wing, there are several constraints that will have to be considered, including:

1. The cost of implementing the solution must be within the budget of the QFSAE team.
2. The solution must be easily replicated by the Queen's formula SAE team.
3. The solution must have no impact on the protection of the driver or structural integrity of the vehicle.
4. The solution must have no significant negative impact on the environment.
5. The solution must be easy to implement on the existing QFSAE vehicle.

Another significant constraint that must be considered for this project are the rules of the Formula SAE competition. The 2022 Formula SAE rules outline that any piece of the car that is not classified as light body work light nose cones or outboard wheel assemblies must be able to resist a standard force impact of 95 kilonewtons [9]. The rules also outlined that any section of the car cannot have a mass greater than 12 kilograms [9]. Thus, the wing can neither be too thin nor too thick so that it complies with both rules.

The triple bottom line factors that will be addressed include the safety of the drivers, which must not be compromised because of modifying the rear wing. The economic effects on the QFSAE Team as there

is more student engagement towards the project. Also, as the vehicles are further optimised and their aerodynamic efficiency is improved, the amount of greenhouse gas emissions will be reduced, thus having a positive environmental impact.

3 Model Description

To approach the problem, it is first necessary to determine the mathematical model for the system. The primary model to study is the fluid dynamics of the airflow around the wing. In addition, the mathematical model is too complex to analytically solve, so it is also required to explore numerical methods for attaining approximate solutions to these models.

3.1 Fluid Mechanics

To model this problem, it is first essential to understand the general theory of fluid mechanics and the governing equations which it gives rise to. The principles of lift, drag and their dependency on shape and Reynolds number will be discussed in this section.

3.1.1 Lift and Drag Forces

Any object moving through a fluid will experience drag, which is a net force in the flow direction as a result of pressure and shear forces acting on the object. The coefficient of drag is expressed in Equation 1:

$$C_D = \frac{2D}{\rho U^2 A} \tag{1}$$

Where, D is the drag force, ρ is the fluid density, U is the upstream velocity, and A is the planform area of the body [2]. Drag can be broken down into two components: friction drag and pressure drag. Friction drag is a result of the shear stress and is a function of the wall shear stress and the orientation of the surface it is acting on [2]. Pressure drag is dependent on the magnitude of the pressure and the orientation of the object. Friction drag accounts for components of the shear force that are parallel to the flow while pressure drag accounts for components of pressure force that are normal to the flow [2].

The drag force is dependent on many properties including shape, Reynolds number, compressibility effects, surface roughness, and Froude number [2]. The drag for different shapes varies from streamlined to blunt bodies. It is assumed that this discussion is limited to incompressible flow on the surface of a smooth object. The Reynolds number also affects the drag coefficient [2]. There are three categories of Reynolds number dependence which are low, moderate, and high Reynolds number flow. First, consider the flow over a smooth sphere. At a low Reynolds number, viscous effects are important in a large area, there is no separation, and the drag coefficient and Reynolds number are linearly related. For Reynolds numbers between 10^3 and $2\text{x}10^5$, viscous effects become important within the boundary layer, and due to the pressure increase, separation begins to occur resulting in wake regions forming downstream. The drag coefficient becomes a constant of 0.4 for the smooth sphere. Finally, for Reynolds numbers greater than $2\text{x}10^5$, the boundary layer becomes thinner in the front of the sphere and begins its transition to turbulent flow [1]. Figure 1 displays the relationship between the Reynolds number and drag coefficient for flow over a smooth sphere [2].

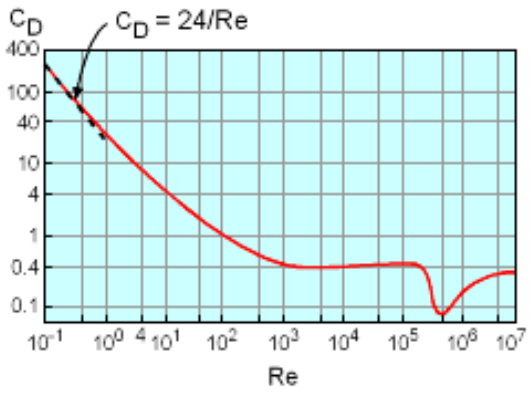

Figure 1: Plot of Reynolds number versus coefficient of drag for flow over a smooth sphere [1].

The drag coefficient varies with bluntness as a function of Reynolds number. Figure 2 shows how the drag coefficient changes for flow over 2-dimensional bodies with varying degrees of streamlining.

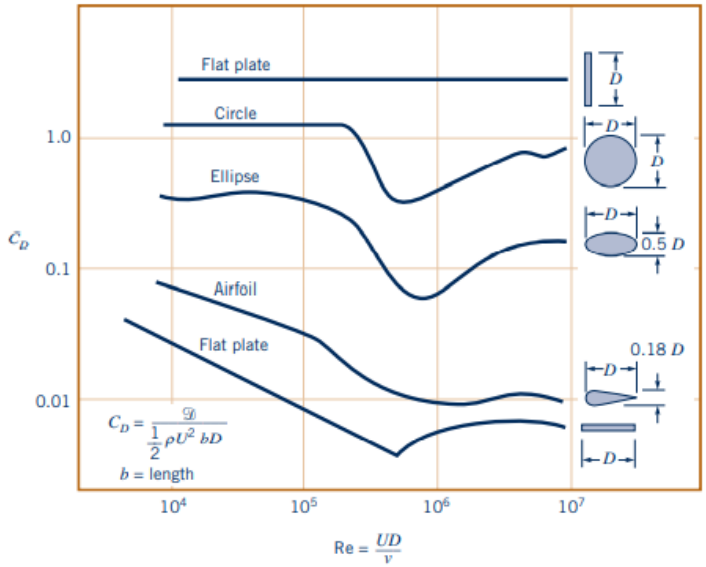

Figure 2: Plot of Reynolds number versus coefficient of drag for flow over different bodies [2].

It is known that any object moving through a fluid will experience a drag force. If this object is not symmetrical there may also be a force normal to the free stream, which is known as the lift [2]. The lift coefficient is given by the relationship outlined in Equation 2.

$$C_L = \frac{L}{\frac{1}{2}\rho U^2 A} \tag{2}$$

Where, L is the lift, ρ is the fluid density, U is the upstream velocity, and A is the planform area [2]. Most lift generating devices, such as airfoils, occur in the large Reynolds number range where there exists a boundary layer in which viscous effects are present. In this case, most of the lift comes from the surface pressure distribution [2]. The QFSAE vehicle can be represented in a free body diagram by Figure 3.

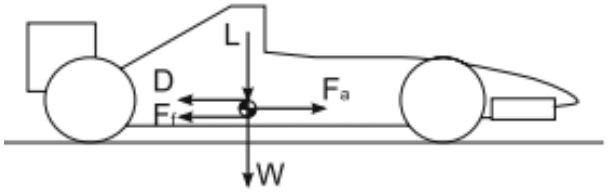

Figure 3: Simplified free body diagram of the QFSAE vehicle [3].

Where, L is the downforce (equal and opposite to the lift). The vehicle can be analyzed on a curved or straight section of its path [3]. For this problem, a section of straight acceleration will be considered. Thus, the total acceleration of the car for a fixed angle of attack of the rear wing is given by Equation 3 [3].

$$a = \frac{F_a - F_f - D}{m} \tag{3}$$

Where, F_a is the force of acceleration given by the engine, F_f is the force of friction on the tires, D is the force of drag, and m is the mass of the car [3]. Assuming the engine acceleration to be constant, the force of friction is given by Equation 4.

$$F_f = \mu[mg + \frac{1}{2}\rho U^2 A C_L] \tag{4}$$

Where, μ is the coefficient of friction on the tires, and g is the acceleration due to gravity. The planform area A is defined by Equation 5.

$$A = bc \tag{5}$$

Where, b is the length of the rear wing which will be modelled as an airfoil and c is the chord length [2]. The drag force is given by Equation 6.

$$D = \frac{1}{2}\rho U^2 C_D A \tag{6}$$

The coefficient of drag of the rear wing is given by Equation 7.

$$C_D = C_{D_0} + \frac{C_L^2}{\pi \text{Æ} e} \tag{7}$$

Where, C_{D_0} is the coefficient of drag for an angle of attack of zero, Æ is the aspect ratio, and e is the Oswald factor, which is a correction factor comparing this wing to an ideal wing of the same aspect ratio [3]. Figure 4 displays the relationship between the angle of attack of the airfoil and the drag coefficient at varying aspect ratios.

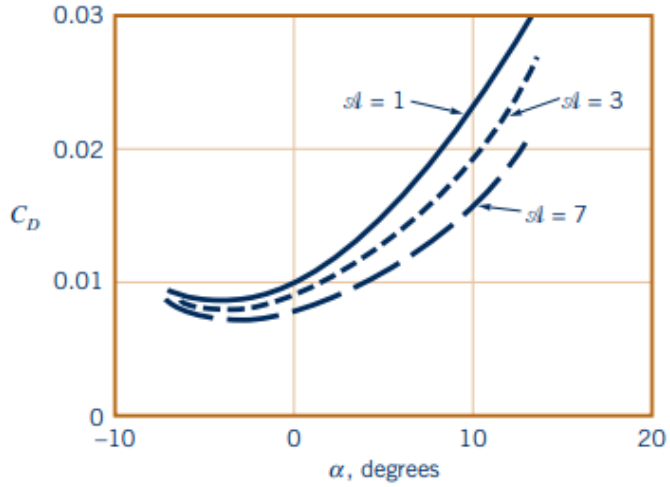

Figure 4: Plot of angle of attack versus drag coefficient for different aspect ratios of an airfoil [2].

Figure 5 displays the relationship between the angle of attack of the airfoil and the lift coefficient at varying aspect ratios.

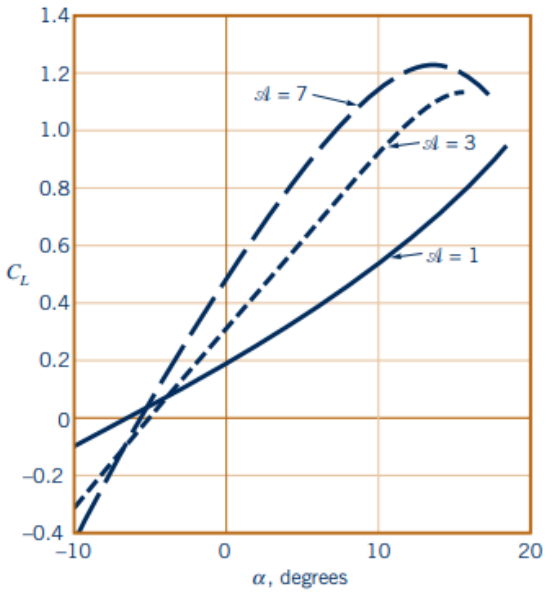

Figure 5: Plot of angle of attack versus lift coefficient for different aspect ratios of an airfoil [2].

There is another fluids phenomenon that is relevant when considering external flows of cars, specifically, the concept of flow separation and its influence on wake. At some points in the flow over the surface, the velocity can stall, resulting in the air around the vehicle moving in the opposite direction. This concept is known as separation, which often results in wake. Wake is a large low pressure turbulent region at the rear of the vehicle. This phenomenon is important to consider as the wake contributes to pressure drag, which negatively impacts vehicle performance [10]. It is important to specify that for the purposes of this project, the discussion will be centered around the rear wing of the QFSAE vehicle, although the entire car and its other components influence the drag force.

3.1.2 Navier-Stokes Equations

To calculate the lift and drag coefficients for this problem, the air pressure and velocity along the surface of the rear wing must be determined. The Navier-Stokes equations allow for this analysis. These equations consist of a continuity equation for conservation of mass, three conservation of momentum equations, and a conservation of energy equation that provide a complete mathematical description of incompressible Newtonian fluids, thus allowing to solve for pressure, density, temperature, and velocity [2] [11]. The differential form of the conservation of mass is the continuity equation displayed in Equation 8 [11].

$$\frac{\partial \rho}{\partial t} + \frac{\partial(\rho u)}{\partial x} + \frac{\partial(\rho v)}{\partial y} + \frac{\partial(\rho w)}{\partial z} = 0 \tag{8}$$

Where, ρ is the fluid density and u, v, and w are the x, y, and z components of the velocity, respectively, as shown in Figure 6.

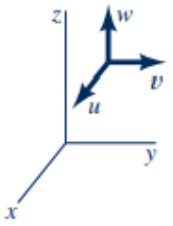

Figure 6: Rectangular coordinate system used to define Navier-Stokes equations [2].

Momentum is defined as the mass of an object multiplied by its velocity. The law of conservation of momentum says that momentum is neither created nor destroyed, but can be changed when forces are involved [12]. The x, y, and z momentum equations are shown in Equation 9 [2].

$$\begin{cases} \rho(\frac{\partial u}{\partial t} + u\frac{\partial u}{\partial x} + v\frac{\partial u}{\partial y} + w\frac{\partial u}{\partial z}) = -\frac{\partial p}{\partial x} + \rho g_x + \mu(\frac{\partial^2 u}{\partial x^2} + \frac{\partial^2 u}{\partial y^2} + \frac{\partial^2 u}{\partial z^2}) \\ \rho(\frac{\partial v}{\partial t} + u\frac{\partial v}{\partial x} + v\frac{\partial v}{\partial y} + w\frac{\partial v}{\partial z}) = -\frac{\partial p}{\partial y} + \rho g_y + \mu(\frac{\partial^2 v}{\partial x^2} + \frac{\partial^2 v}{\partial y^2} + \frac{\partial^2 v}{\partial z^2}) \\ \rho(\frac{\partial w}{\partial t} + u\frac{\partial w}{\partial x} + v\frac{\partial w}{\partial y} + w\frac{\partial w}{\partial z}) = -\frac{\partial p}{\partial z} + \rho g_z + \mu(\frac{\partial^2 w}{\partial x^2} + \frac{\partial^2 w}{\partial y^2} + \frac{\partial^2 w}{\partial z^2}) \end{cases} \tag{9}$$

Where, p is the pressure and g_x, g_y, and g_z are the x, y, and z components of acceleration due to gravity. The conservation of energy can be expressed as represented in Equation 10 [11].

$$\begin{aligned} &\frac{\partial(E_T)}{\partial t} + \frac{\partial(uE_T)}{\partial x} + \frac{\partial(vE_T)}{\partial y} + \frac{\partial(wE_T)}{\partial z} \\ &= -\frac{\partial(up)}{\partial x} - \frac{\partial(vp)}{\partial y} - \frac{\partial(wp)}{\partial z} - \frac{1}{RePr}(\frac{\partial q_x}{\partial x} + \frac{\partial q_y}{\partial y} + \frac{\partial q_z}{\partial z}) \\ &\quad + \frac{1}{Re}(\frac{\partial}{\partial x}(u\tau_{xx} + v\tau_{xy} + w\tau_{xz}) + \frac{\partial}{\partial y}(u\tau_{xy} + v\tau_{yy} + w\tau_{yz}) + \frac{\partial}{\partial z}(u\tau_{xz} + v\tau_{yz} + w\tau_{zz})) \end{aligned} \tag{10}$$

Where, E_t is the total energy, Re is the Reynolds number, Pr is the Prandtl number, q is the heat flux and τ is the shear stress. Equations 8 to 10 construct the Navier-Stokes equations. Since these equations are non-linear, second order, partial differential equations, there is no direct solution for turbulent flow [2].

3.1.3 Assumptions

The following assumptions have been made for the flow around the rear wing of the QFSAE vehicle. A 3-dimensional, steady state, incompressible, turbulent flow is assumed [13]. Also, it is assumed that viscous effects are limited to the boundary layer and outside the boundary layer is inviscid flow [10]. 3-dimensional

flow implies that the x, y, z coordinate system will be used. Steady flow refers to flow in which the velocity is independent of time, or as shown in Equation 11 [2].

$$\frac{\partial U}{\partial t} = 0 \tag{11}$$

Incompressible flow means that the density is constant as expressed in Equation 12.

$$\frac{\partial \rho}{\partial t} = 0 \tag{12}$$

Turbulent flow means the Reynolds number is greater than 3500 for external flows [14].

3.2 Numerical Analysis

It is generally not possible to solve the equations governing fluid dynamics analytically, due to the nature of the second order partial differential equations which arise in the Navier Stokes equations, compounded with the additional complex turbulence models implemented in the system. To practically solve for the fluid velocity and pressure, it is necessary to use numerical methods to approximate the solutions to the system.

3.2.1 Reynolds-Averaged Navier-Stokes (RANS)

RANS is a common numerical method for analysing the Navier-Stokes equations. This method involves quantizing the continuous space regions into discrete averages, converting the system into a discrete problem which can be solved through a sequence of discrete computations. Under the assumptions that the fluid is steady-state and incompressible, the system of equations governing RANS is shown below in Equation 13 [15].

$$\begin{cases} (\mathbf{v} \cdot \nabla)\mathbf{v} = -\nabla p + \nabla \cdot (2v\mathrm{D}(\mathbf{v})) - \alpha \mathbf{v} \\ \nabla \cdot \mathbf{v} = 0 \end{cases} \tag{13}$$

In the above equations, $\mathbf{v}$ represents the velocity of the fluid, p represents the pressure, and α represents the porosity distribution. The notable difference between these equations and the original Navier-Stokes equations is the introduction of the porosity, which is used to account for the inaccuracies which are introduced from discretizing the system.

3.2.2 Turbulence Models

From the RANS equations, different turbulence models can be derived based on the way in which the Reynolds stress is modelled. Some examples of common turbulence models include Standard K-ω, K-ϵ, and Spalart-Allmaras models. The advantages and disadvantages of these three turbulence models are considered in Tables 1 and 2 [4].

Table 1: Advantages of the Standard K-ω, K-ϵ and Spalart-Allmaras models.

K-ω	K-ϵ	Spalart-Allmaras
Good for external flows	Good for external flows	Fast implementation
Strong vortices	Reasonable accuracy	Good convergence
No wall function necessary		Forgiving of poor quality mesh

Table 2: Disadvantages of the Standard K-ω, K-ϵ and Spalart-Allmaras models.

K-ω	K-ϵ	Spalart-Allmaras
Over-predicts shear stress	Wall functions are necessary	No wall functions
Over-predicts separation	Poor performance for flows with separation	Not good for shear flows
Difficulty converging		Under-predicts separation

The Standard K-ω turbulence model was selected for this project due to its common application to external aerodynamics, strong vortices, and that no wall function is necessary. This works well for the selected application as this turbulence model is already implemented into the fluids modelling software that will be used. Also, the K-ω turbulence model is currently used by the QFSAE team [16]. Figure 7 illustrates a simulated model of a car under the K-ω turbulence model.

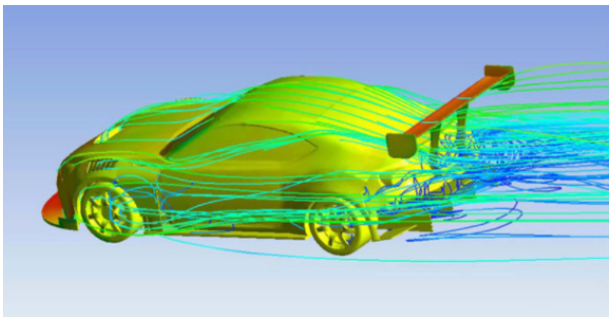

Figure 7: Simulated model of a car under the K-ω turbulence model [4].

The two-equation model is given by Equation 14 [17].

$$\begin{cases} \frac{\partial(\rho k)}{\partial t} + \frac{\partial(\rho u_j k)}{\partial x_j} = P - \beta^* \rho \omega k + \frac{\partial}{\partial x_j}((\mu + \sigma_k \frac{\rho k}{\omega})\frac{\partial k}{\partial x_j}) \\ \frac{\partial(\rho \omega)}{\partial t} + \frac{\partial(\rho u_j \omega)}{\partial x_j} = \frac{\gamma \omega}{k} P - \beta \rho \omega^2 + \frac{\partial}{\partial x_j}((\mu + \sigma_\omega \frac{\rho \omega}{\omega})\frac{\partial \omega}{\partial x_j}) + \frac{\rho \sigma_d}{\omega}\frac{\partial k}{\partial x_j}\frac{\partial \omega}{\partial x_j} \end{cases} \tag{14}$$

The turbulent eddy viscosity is computed using Equation 15 [17].

$$\mu_t = \frac{\rho k}{\hat{\omega}} \tag{15}$$

Where, ρ is the density, μ is the molecular dynamic viscosity, and k is the turbulent kinetic energy. $\hat{\omega}$ is the specific turbulence dissipation, which determines the rate of dissipation per unit of kinetic energy as defined in Equation 16 [18].

$$\hat{\omega} = max[\omega, C_{lim}\sqrt{\frac{2\overline{S}_{ij}\overline{S}_{ij}}{\beta^*}}] \tag{16}$$

where

$$\overline{S}_{ij} = S_{ij} - \frac{1}{3}\frac{\partial u_k}{\partial x_k}\delta_{ij} \tag{17}$$

The constants and auxiliary functions are provided below.

$$\sigma_k = 0.6 \quad \sigma_\omega = 0.5 \quad \beta^* = 0.09 \quad \gamma = \frac{13}{25} \quad C_{lim} = \frac{7}{8} \quad \beta = \beta_0 f_\beta \quad \beta_0 = 0.0708 \quad f_\beta = \frac{1 + 85\chi_\omega}{1 + 100\chi_\omega}$$

$$\chi_\omega = |\frac{\Omega_{ij}\Omega_{jk}\hat{S}_{ki}}{(\beta^*\omega)^3}| \qquad \hat{S}_{ki} = S_{ki} - \frac{1}{2}\frac{\partial u_m}{\partial x_m}\delta_{ki} \qquad \Omega_{ij} = \frac{1}{2}(\frac{\partial u_i}{\partial x_j} - \frac{\partial u_j}{\partial x_i}) \qquad \begin{cases} \sigma_d = 0, for(\frac{\partial k}{\partial x_j}\frac{\partial \omega}{\partial x_j}) \leq 0 \\ \sigma_d = \frac{1}{8}, for(\frac{\partial k}{\partial x_j}\frac{\partial \omega}{\partial x_j}) > 0 \end{cases}$$

3.2.3 Computational Fluid Dynamics (CFD)

CFD is the process of using computer programs to estimate the solutions to the Navier-Stokes equations by implementing a numerical method, such as RANS. CFD will be used to produce all numerical results for this project, when analysing the mathematical model of the fluid dynamics. Using computers to perform the discrete computations required in the numerical approximations of fluid dynamics can still take a long time to compute, as the number of computations scales with respect to how fine the divisions of space are. However, using smaller regions leads to more accurate approximations, so there is a trade-off between computation time and accuracy when using CFD. The general process for CFD is that the program will take various properties about the model, fluid, and initial conditions as inputs to produce the field of fluid velocity and pressure as the output. A common way to visualize this data is as a colour map on the surface of the object being analyzed, where more intense colour will typically correspond to larger magnitude values at those points. The output of these programs can be further processed to calculate the drag and lift coefficients for the model under the field that has been generated.

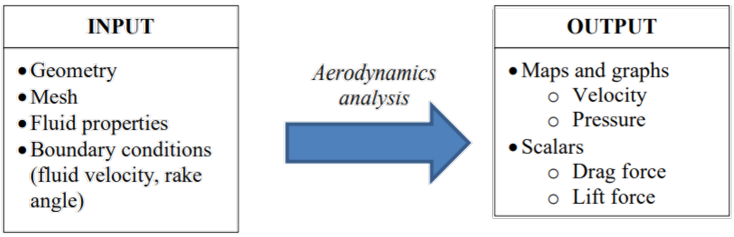

Figure 8: A graphic describing the input/output behaviour of CFD

Since the goal of this project is to optimise the coefficient of drag over all shapes of the rear wing, CFD can be used to compare the coefficient of drag for various shape designs. However, given the high computational cost of running these simulations, and the large set of possible changes that can be made to the shape of a model, it is not possible to perform this analysis on any subset of possible shapes that will deduce optimality. Hence, to practically work toward this optimisation, a more strategic optimisation technique will need to applied.

3.2.4 Adjoint Optimisation

Adjoint optimisation is a technique which reduces the problem of shape optimisation into an iterative process which determines the optimal modifications to make to a given shape, without needing to exhaustively search all possible geometries. The first step in adjoint optimisation is to define a cost function which is calculated at each point on the model's surface, using the fluid velocity and pressure fields. Calculating the gradient of this cost function with respect to the normal displacement at each point on the model yields the optimal direction to deform the surface. After performing the optimal deformations to the model, this process can be repeated until the model converges to an optimal shape.

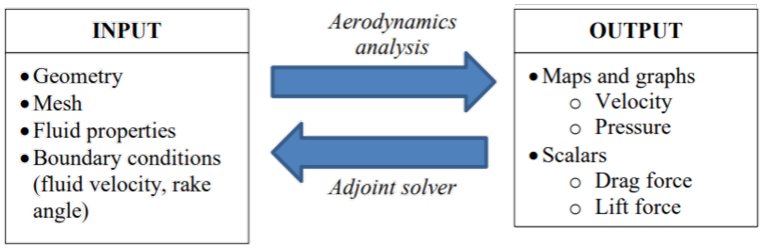

Figure 9: A graphic describing the input/output behaviour of the adjoint optimisation method

To optimise the wing design, the cost function will be a weighted combination of the drag and lift forces, which are directly related to their respective coefficients being optimised. A detailed description of the cost function used in this project is given in Section 4.2. In general, the cost function for an adjoint optimisation will take the following form, shown below in Equation 18 [15].

$$J = \int_{\Gamma} J_{\Gamma}\, d\Gamma + \int_{\Omega} J_{\Omega}\, d\Omega \tag{18}$$

Where in the above equation the cost function is represented as the sum of two integrals: a surface integral over the boundary Γ, and a volume integral over the interior of the domain Ω. For the rear wing optimisation, the boundary Γ is the surface of the wing, and the bounding box in which the simulation is enclosed, while the interior Ω is the volume between the wing and the bounding box. A two dimensional representation of this is shown below in Figure 10.

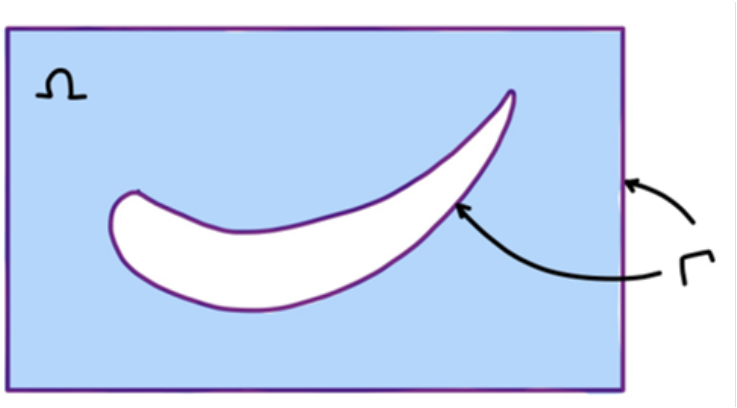

Figure 10: A 2-D representation of the boundary and interior regions for the rear wing optimisation

To calculate the gradient of the cost function in an adjoint optimisation, it is first necessary to construct and solve a different set of fluid dynamic equations, called the adjoint field equations. This new system is governed by the following set of equations, shown below in Equation 19 [15].

$$\begin{cases} (\mathbf{v}\cdot\nabla)\mathbf{u} - \nabla\mathbf{u}\cdot\mathbf{v} = -\nabla q + \nabla\cdot(2v\mathrm{D}(\mathbf{u})) - \alpha\mathbf{u} - \frac{\partial J_{\Omega}}{\partial \mathbf{v}} \\ \nabla\cdot\mathbf{u} = \frac{\partial J_{\Omega}}{\partial p} \end{cases} \tag{19}$$

With the boundary conditions:

$$\mathbf{n}\cdot\nabla q = 0 \qquad \mathbf{u}_t = 0 \qquad u_n = -\frac{\partial J_{\Gamma}}{\partial p}$$

Solving the adjoint field equations involves solving for $\mathbf{u}$ and q which are called the adjoint velocity and pressure, respectively. It is assumed that the fluid velocity and pressure ($\mathbf{v}$ and p) have already been calculated, while J_{Ω} and J_{Γ} are the components of the adjoint cost function as expressed in the form of Equation 18. After solving for $\mathbf{u}$ and q, the gradient of the cost function is calculated as follows [15]:

$$\frac{\partial J}{\partial \alpha} = \mathbf{u}\cdot\mathbf{v} \qquad \frac{\partial J}{\partial \beta} = -v\partial_n\mathbf{u}\cdot\partial_n\mathbf{v}$$

Where α is the porosity, and β is displacement in the direction normal to the surface. For adjoint shape optimisation, the sensitivity in the normal direction is analyzed to make the iterative changes to the model to optimise the cost function.

4 Model Implementation

With the mathematical model developed, the focus is now shifted to model implementation. As mentioned in Section 3, the mathematical model for this problem is, in general, impossible to solve analytically. As such, numerical methods and CFD software must be used to generate solutions. In this section, the software of choice will be introduced, and the method for implementing these numerical methods will be further discussed.

4.1 Software and Tools

The majority of the modelling conducted for this project is done using a tool called OpenFOAM CFD (Open-source Field Operation And Manipulation) [19]. OpenFOAM is a free open-source C++ toolbox used by Queen's Formula SAE team, as well as many professionals in the industry. The OpenFOAM toolbox contains a rich variety of solvers and resources used for fluid dynamics applications. The solvers used to model the airflow around the rear wing and the adjoint optimisation method are called *simpleFoam* [20] and *adjointOptimisationFoam* [21] respectively. All construction and adjustments made to 3D models of the rear wing are performed using SolidWorks [22], and the results of the OpenFOAM simulation is displayed using ParaView [23].

4.2 The Adjoint Optimisation Model in OpenFOAM

simpleFoam is OpenFOAM's default steady-state solver for finite volume, incompressible, turbulent flow. The solver makes use of the Semi-Implicit Method for Pressure Linked Equations (SIMPLE) algorithm [24] to solve the equations for the velocity ($\mathbf{u}$) and pressure ($\mathbf{p}$) of the airflow around an object. *simpleFoam* makes use of the RANS quantization, and use of the K-ω turbulence model can be specified.

adjointOptimisationFoam builds off the *simpleFoam* solver - solving for $\mathbf{u}$ and $\mathbf{p}$ in the same way, while additionally solving the adjoint field equations 19 described in 3.2.4. The critical information used by the adjoint solver is specified in the `optimisationDict` dictionary. Listing 1 shows the code snippet used to define the cost function. This tells the solver precisely what quantities to optimise under which conditions. In this case, there are two objectives to optimise over; lift and drag. For each objective, the first line specifies its weight towards the cost function. In this example lift will contribute 25% towards the cost function, while drag contributes the remaining 75%. In the next line the type of objective is specified. Both lift and drag are forces, this informs OpenFOAM what form the cost function will take for each objective. The cost function for a force is described by Equation 20.

$$J = \frac{\int_{S_W} \rho(\tau_{ij} n_j + p n_i) r_i \, dS)}{\frac{1}{2}\rho A U_\infty^2} \tag{20}$$

Here τ_{ij} are the components of the stress tensor. p is the pressure divided by the constant freestream density ρ. n is the unit normal vector and r defines the direction in which the force vector should be projected. S_W are the wall surfaces on which force is defined, i.e the object to be optimised. A is the reference area of the object, in general this is the cross-sectional frontal area of the object, however, for an airfoil it is the nominal wing area (Wing length $\times$ Wing chord). Finally, U_∞ is the airflow velocity magnitude. The remaining fields in the objective specify the values of the constants used in the cost function. Lift will be projected in the positive z direction and drag is projected in the positive x direction. At this point, it is important to note that the airflow is specified to travel in the positive x direction, so these quantities make sense. Aref (A) is set at 1, Rhoinf (ρ) is set to the freestream density of dry air at sea level ($1.225 \frac{\text{kg}}{\text{m}^3}$) [25], and UInf ($U_\infty$) is set to $25 \frac{\text{m}}{\text{s}}$.

```
objectiveNames
{
    lift
    {
        weight      0.25;
        type        force;
        patches     (RW);
```

```
        direction   (0 0 1);
        Aref        1;
        rhoInf      1.225;
        UInf        25;
    }
    drag
    {
        weight      0.75;
        type        force;
        patches     (RW);
        direction   (1 0 0);
        Aref        1;
        rhoInf      1.225;
        UInf        25;
    }
}
```

Listing 1: Snippet of `optimisationDict` used to define the cost function.

Another important item in the `optimisationDict` is the optimisation manager. Here the options are `singleRun` and `steadyOptimisation`. When the optimisation manager is in `singleRun` mode, the primal (the RANS flow equations under the K-ω turbulence model) and adjoint equations are iterated either until the residual values have been achieved or the max number of iterations have been reached. In this process, the primal and adjoint equations are solved just once, then the sensitivities are reported. When in `steadyOptimisation` mode, the simulation iterates through the `singleRun` process, applying a small change to the mesh on each iteration, based on the sensitivities. For simplicity, and limitations to computational power, the optimisation manager will be set to `singleRun` for this project. The full `optimisationDict` listing can be found in Appendix A.

Figure 11 shows the process used by the *adjointOptimisationFoam* solver in `singleRun` mode. First, the initial conditions and design variables are defined. This includes both the boundary and internal mesh, as well as choosing the turbulence model, and flow velocity. Then the primal system is solved, and the cost J is computed at that time instant. Then, the adjoint system is solved, i.e. the adjoint field equations 19, and the adjoint sensitivities of each cell in the mesh are computed and updated as a gradient of the cost function using the steepest descent method. Then, the program checks to see if it has met the terminal condition, either the stop time has been reached, or the residuals have converged (i.e. the difference between the observed and expected adjoint pressure and adjoint velocity is less than some small ϵ). If it does meet the terminal condition, it exits and report the final sensitivity values for each cell. If not, it will increment the time and iterate through the same process.

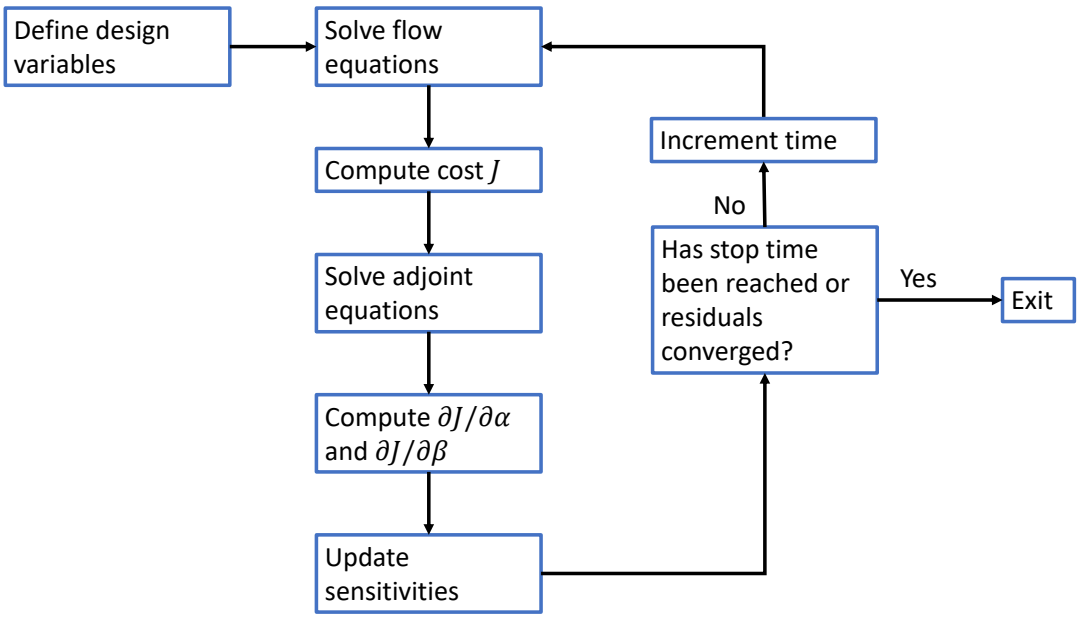

Figure 11: Flowchart showing the process used by the *adjointOptimisationFoam* solver in `singleRun` mode.

5 Model Validation

The adjoint shape optimisation algorithm implemented using OpenFOAM must first be validated before being applied to the rear wing. The legitimacy of the assumptions made and the model results is verified by applying the solver to well documented geometries such as a cube and sphere. For validation purposes, the cost function will be minimizing the coefficient of drag (C_D), and will ignore optimisation over lift. This is done to simplify the validation process, and ensures the results will be straightforward to visually confirm. Indeed, it is easy to picture a more aerodynamic and streamlined version of a shape, rather than attempting to imagine the perfect balance between lift and drag.

The coefficients of drag provided by the model are then be compared to the known values for that specific shape. As mentioned in Section 3, drag coefficients are not constant, and depend on airflow and Reynolds number - which in turn is a function of A, ρ and U_∞. These values have been selected in the definition of the cost function to closely match the Reynolds number of the comparison shape ($\approx 10^5 - 10^6$). As such, the objective of this validation will be to ensure that the absolute values of C_D are within a reasonable range of the known values, then focus on the relative values between the drag coefficients, rather than the absolute values.

The shapes are then modified using SolidWorks based on the resulting sensitivity map provided at the end of the OpenFOAM simulation. The cells of the mesh will be coloured blue if displacing that cell inward normal to the surface will reduce the cost function, and red if moving that cell outward normal to the surface will reduce the cost function. These new 3D models, with the suggested changes are then tested once again with the expectation that the coefficient of drag will be reduced with each iteration. A summary of the validation results can be found in Table 3.

Table 3: Comparison of the coefficient of drag between known values and OpenFOAM model results.

$\mathbf{C_D}$	Known Value [26]	Simulation Value	First Iteration	Second Iteration
Cube	1.05	1.099	0.77	0.65
Sphere	0.1	0.105	0.0847	0.0638

Figure 12 shows the resulting sensitivity maps for a cube and sphere with side length (or diameter) 1mm after the *adjointOptimisationFoam* simulation. Notably, the observed drag coefficients for both shapes are within 5% of the expected value. First, observing the cube, the most obvious feature is the dark blue border on the edges of the front face. This suggests that those cells should be pushed inwards. Intuitively, this is an expected result, as seems this modification would streamline the shape. Less noticeable in Figure 12, is a red line on the edge of the rear face, shown more clearly in Figure 13. For the first iteration of modifications to the cube, a 0.05mm fillet is added to the edges on the front face. The red on the back is ignored for now, to isolate the effects on C_D for each modification made to the 3D model.

The sphere has a more complex sensitivity map. However, the general trend suggests pushing the cells in the front half of the sphere inwards, and stretching the cells on the back half outward. These changes are more difficult to add to the 3D model of the sphere, so a new shape is created using a circle as a template. Figure 14 shows a cross-section of the modified shape overlaid on a circle. Lines are drawn 30° in front and behind the vertical mid line of the circle. The line in front is 0.025mm shorter than the 0.5mm radius of the base circle, while the back line is 0.025mm longer. Knowing that the sensitivity map shows local changes, the back of the circle is drawn out to account for the movement of the other cells in the geometry. The points at the end of these lines are then joined with a spline tool. This 2D geometry is then revolved around its horizontal axis, resulting in a sphere-like shape with 0.5mm radius deformed in the way the sensitivity map suggests.

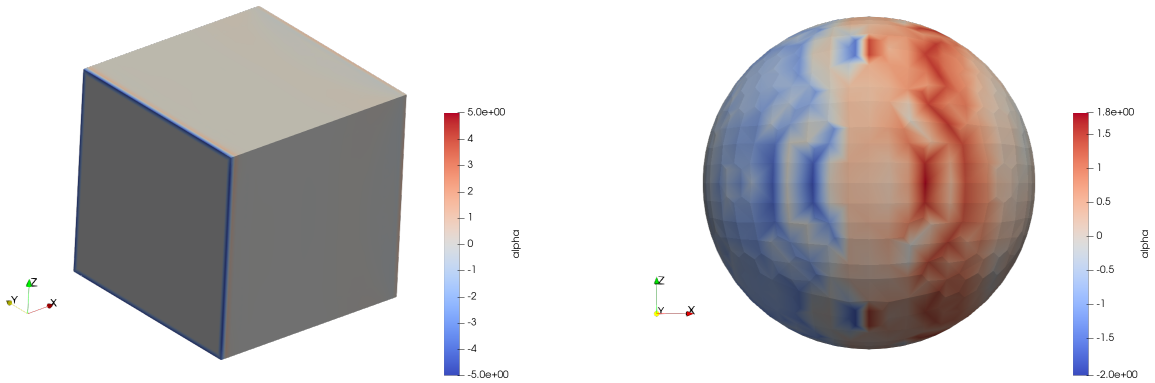

(a) Cube: $C_D = 1.099$ (b) Sphere: $C_D = 0.105$

Figure 12: Sensitivity map of first iteration of adjoint modelling.

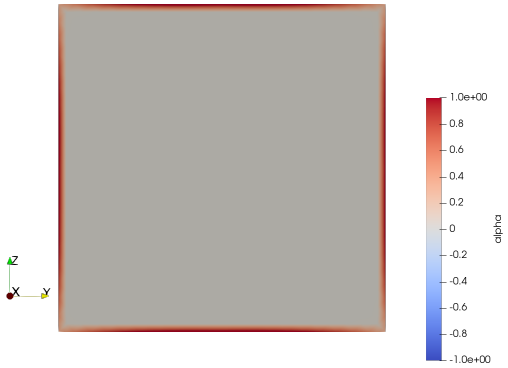

Figure 13: A rear view of the cube sensitivity map, showing red on the back edges.

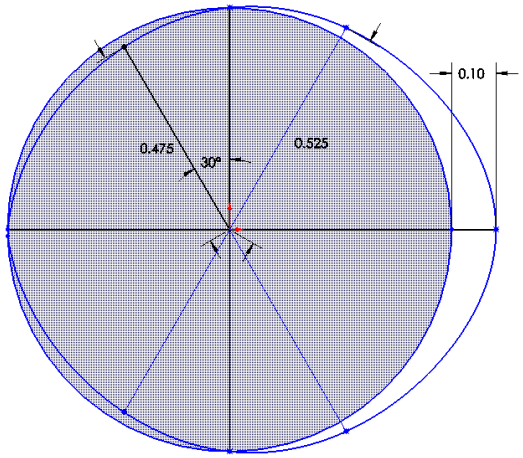

Figure 14: A diagram showing the method used to make modifications to the sphere.

Figure 15 shows the results of the adjoint optimisation on the new geometries. The cube saw a reduction in C_D of $\approx 30\%$, while the sphere's C_D was reduced by $\approx 20\%$. However, the sensitivity map shows that there are still improvements to be made. For the final iteration of the cube, the red features on the rear edges will be addressed. Observing Figure 13 carefully, the sensitivity is is most intense at the midpoint of the edge, and tapers off towards the corners. This implies that more material should be added around the middle, and almost no material should be added around the corners. Figure 16 shows the 2D curve which will be revolved around each edge of the back face. The sensitivity map for the sphere continues to suggest the same changes as before. Thus, the changes made it Figure 14 will be made more extreme.

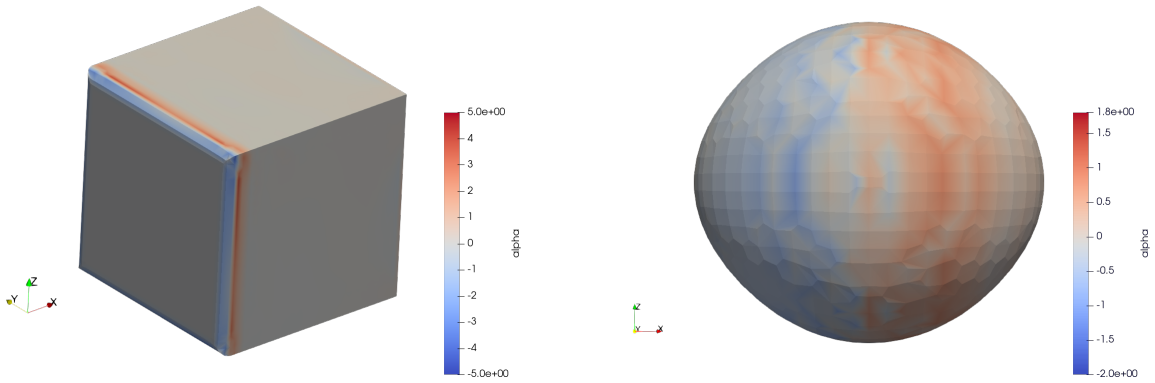

(a) Cube: $C_D = 0.77$

(b) Sphere: $C_D = 0.00847$

Figure 15: Sensitivity map of second iteration of adjoint modelling.

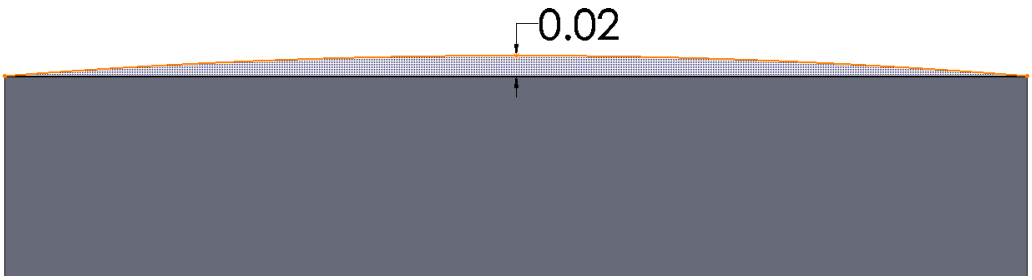

Figure 16: A diagram showing the method used to make modifications to the cube.

Finally, Figure 17 shows the third and final iteration of the validation shapes. Once again a reduction in drag is observed, with the modified cube down an additional $\approx 16\%$, and the sphere down $\approx 25\%$ for a total reduction in C_D of $\approx 41\%$ and $\approx 39\%$ respectively. The results of these simulations confirm that the model works as expected. Furthermore, both shapes look more streamlined which visually confirms the results of the model. Therefore, with the model now validated, it can now be applied towards optimising the shape of the rear wing.

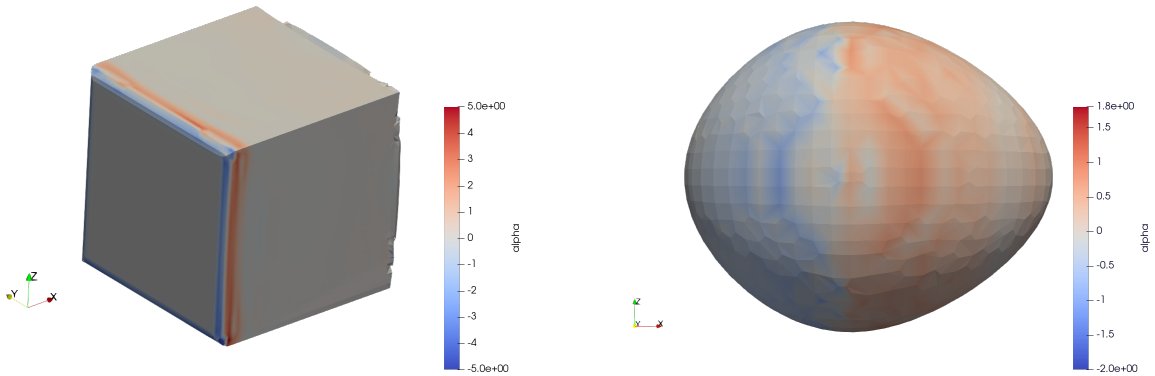

(a) Cube: $C_D = 0.65$ (b) Sphere: $C_D = 0.0638$

Figure 17: Sensitivity map of third iteration of adjoint modelling.

6 Results

The same process used in the validation step was used to analyze the current rear wing model of the QFSAE car, and apply the adjoint optimisation process to achieve the goals set out for this project.

6.1 Rear Wing Results

As with the simple validation shapes, the first step in the analysis was to validate the fluid dynamic model being used by OpenFOAM to analyze the rear wing. This was done by using a standard OpenFOAM simulation to calculate the drag and lift coefficients of the wing, then compare them to the validation data received from the QFSAE team. The results of this simulation are shown below. Figure 18 shows the resulting pressure distribution on the wing while Table 4 displays the coefficients calculated by the simulation.

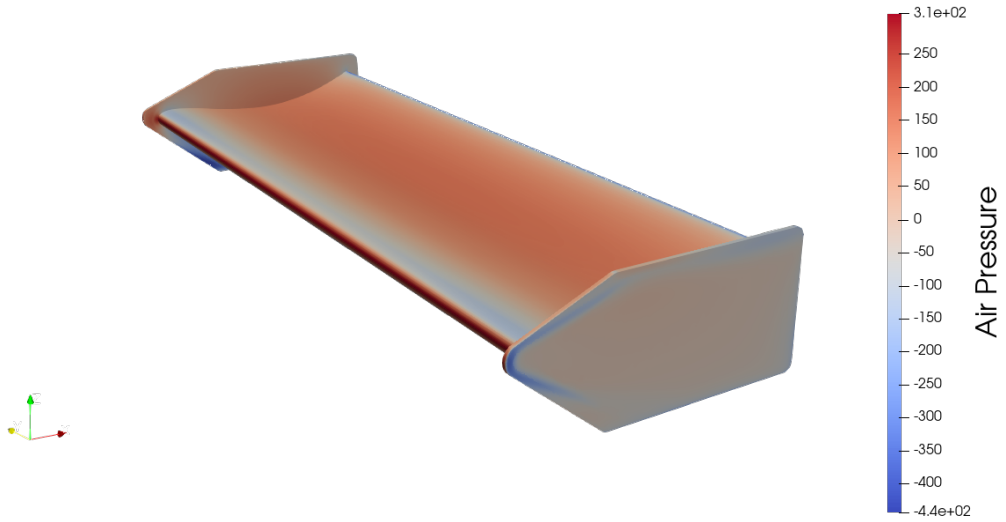

Figure 18: Pressure map on the rear wing generated by OpenFOAM simulation

Table 4: Comparison of coefficients given by OpenFOAM to QFSAE validation data

Coefficient	OpenFOAM	QFSAE [16]	Difference
Drag	0.0338	0.03478	2.8%
Lift	-0.289	-0.2949	2.0%

The coefficients calculated by the OpenFOAM simulation were within a few percent accuracy to the QFSAE data, which validated the OpenFOAM model to be used for optimisation of the wing. For all future results of OpenFOAM simulations on the wing, the coefficients will be compared to the base results of the original wing from OpenFOAM, not the QFSAE values. This was done to prevent biasing the results from the original difference in values.

6.2 Rear Wing Adjoint

The first step in performing an adjoint shape optimisation on the rear wing was to define the cost function to optimise over. This was done using OpenFOAM, so the resulting cost function has the same form as detailed in Section 4.2. The weightings of the cost function for this optimisation were set to 0.75 for drag and 0.25 for lift. This was chosen to ensure more focus on reducing the drag coefficient, while also penalizing increases of the lift coefficient, which hinder performance of the vehicle. The resulting sensitivity map of the adjoint optimisation is shown below in Figure 19.

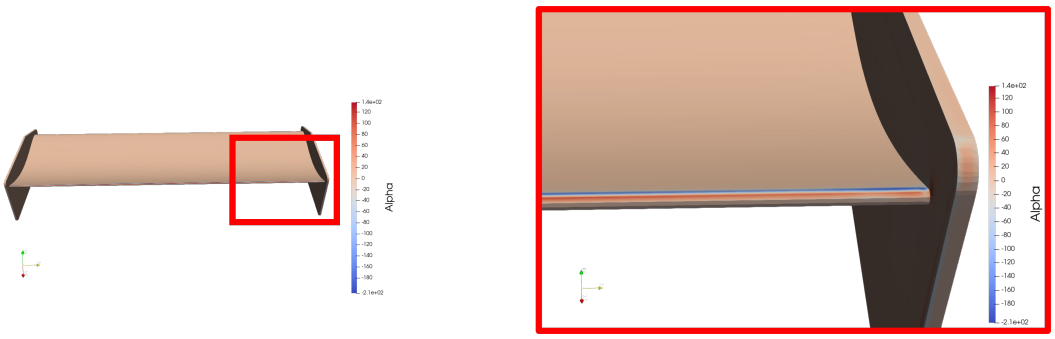

Figure 19: Sensitivity map from adjoint optimisation of rear wing model

Observing this sensitivity maps implies the following areas should be modified to optimise the wing with respect to the chosen cost function. First, the largest magnitude sensitivities were found on the back of the airfoil shape of the wing. The sensitivity shows a negative gradient (blue) above and a positive gradient (red) below. This implies that the tail of the wing should be extended outwards, and made thinner. The other area of interest is the corners of the supporting side structures of the wing. the primarily red colour on the rounded corners suggests these features have too large of a radius, and should be reduced. Also, there were no markings on the front profile of the wing, so no changes should be made to that region.

6.3 Rear Wing Modifications

A SolidWorks drawing of the original model of the rear wing is shown in Figure 20 below, with the top, front, and right views and the associated relevant dimensions labelled in millimeters. Note that the rear wing model was provided by QFSAE and has a 500:1 scale to the physical model [16].

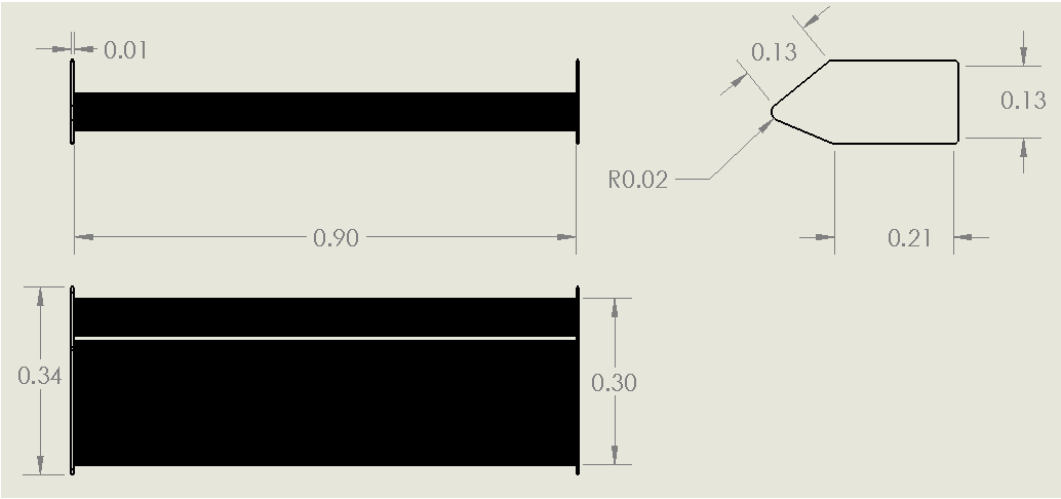

Figure 20: CAD drawing of original rear wing with all relevant dimensions in mm.

After collecting the sensitivity map data from OpenFOAM, the geometry of the rear wing was edited using SolidWorks CAD software. These changes are summarized in three different trial models. The first model was modified to add material to the tail of the wing using a circular addition with radius 0.002mm and make the tail thinner using a 1mm fillet. The side structures were also altered to have 0.001mm fillets applied around all edges. These changes are displayed in Figures 21 to 23.

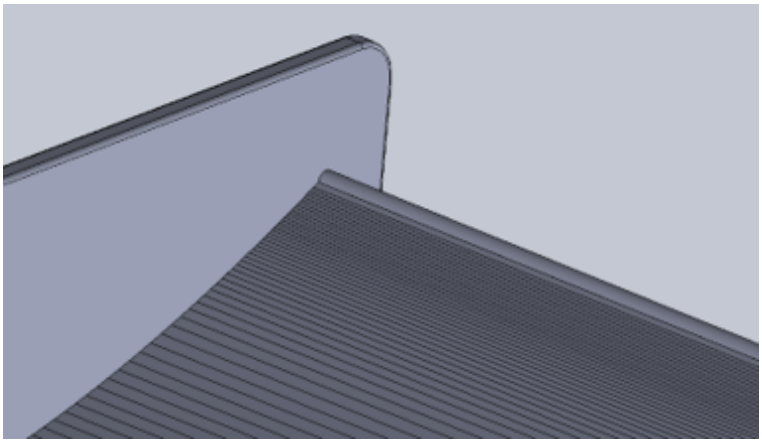

Figure 21: Trial 1 modified rear wing with added fillet, circular addition, and rounded edges of side supports.

Figure 22: Trial 1 modified rear wing cross section of airfoil with added fillet, circular addition, and rounded edges of side supports.

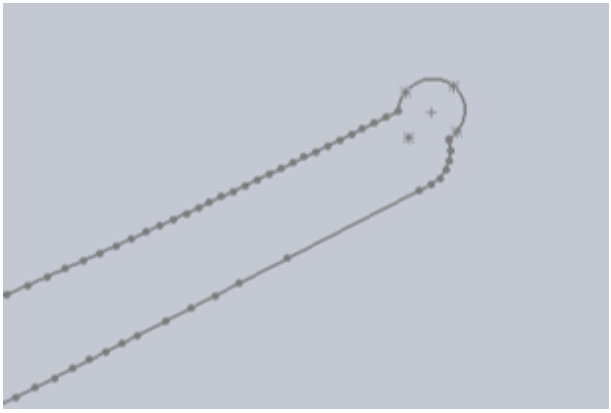

Figure 23: Trial 1 modified rear wing close up cross section of airfoil with added fillet, circular addition, and rounded edges of side supports.

In subsequent trials, the changes made were less extreme. For the second trial, some of the previous changes were removed while the 1mm fillet near the tail of the airfoil was kept, as this was the main area highlighted by the OpenFOAM sensitivity map. The geometry is shown in Figures 24 to 26.

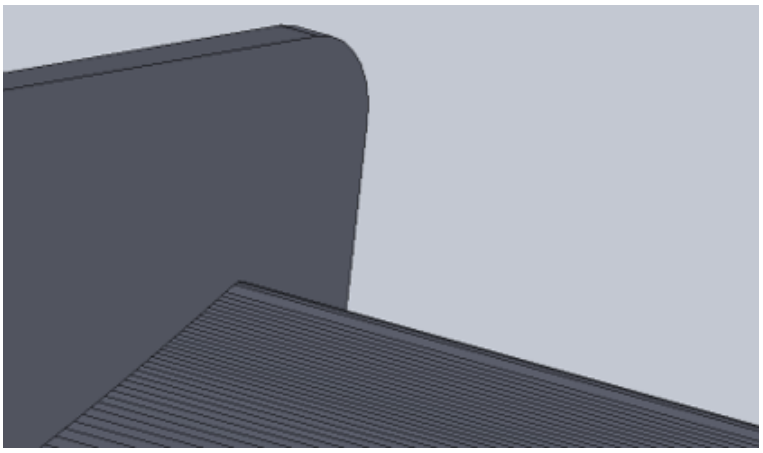

Figure 24: Trial 2 modified rear wing with added fillet.

Figure 25: Trial 2 modified rear wing cross section of airfoil with added fillet.

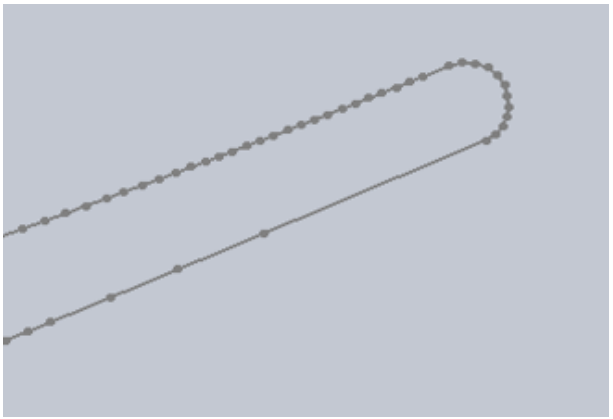

Figure 26: Trial 2 modified rear wing close up cross section of airfoil with added fillet.

Finally, the third trial used an ellipsoid addition with semi-major length 0.0045 mm and semi-minor length 0.002 mm at the tail of the airfoil. Different views of the model are displayed in Figures 27 to 29.

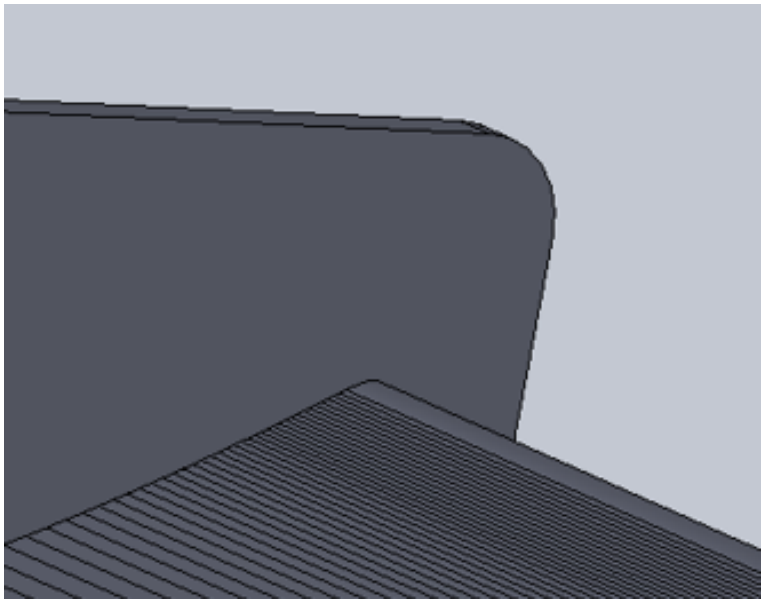

Figure 27: Trial 3 modified rear wing with added ellipse.

Figure 28: Trial 3 modified rear wing cross section of airfoil with added ellipse.

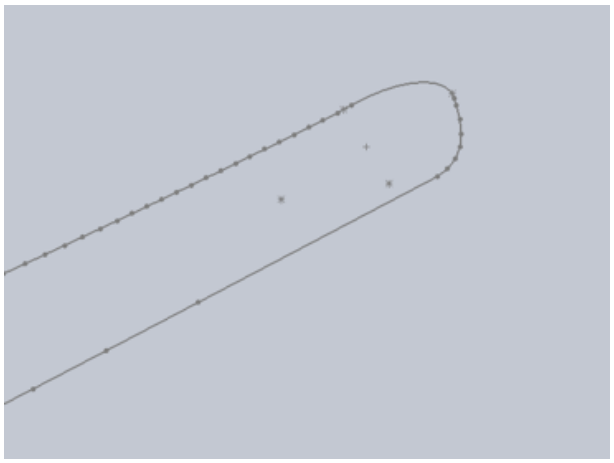

Figure 29: Trial 3 modified rear wing close up cross section of airfoil with added ellipse.

6.4 Model Comparison

Each of the modified models was analyzed using the same OpenFOAM simulation used on the original rear wing model. Their performance was analyzed by comparing the resulting coefficients of lift and drag computed by the simulation to the respective values that were obtained from the original model. The results of this comparison are shown below in Table 5

Table 5: Comparison of the performance of the wing modifications to the original model

Wing Model	Drag Coefficient	Lift Coefficient
Original	0.0338	-0.289
Trial 1	0.0425	-0.329
Trial 2	0.0371	-0.305
Trial 3	0.0326	-0.284

The first observation about these results was the presence of the expected trade-off between drag and lift. This is shown by the models which were calculated to have lower coefficients of drag had larger coefficients of lift, and higher drag implies lower lift. This aligns with the expectation that to minimize drag, the downforce will be affected negatively. The results of this analysis revealed that the models for Trial 1 and 2 both performed worse than the original model, by having a higher coefficient of drag. However, the model for Trial 3 performed slightly better than the original, with a 3.5% reduction to the coefficient of drag, while only increasing the coefficient of lift by 1.8%. The notable differences between these models is that for Trial 3, the least significant changes were made compared to the original, where Trials 1 and 2 have larger changes. Although the drag improvement from Trial 3 did not meet the 5% reduction goal set for this project, given that the changes for Trial 3 were very small, and any larger changes in accordance with the sensitivity map would cause adverse results, it was apparent that the wing design at this point was possibly optimal in terms of the adjoint optimisation.

6.5 Model Optimality

To ensure that the Trial 3 wing was indeed the optimial design, an OpenFOAM adjoint optimisation with identical cost function to the original was performed on this new model. The sensitivity map resulting from this simulation is shown below in Figure 30.

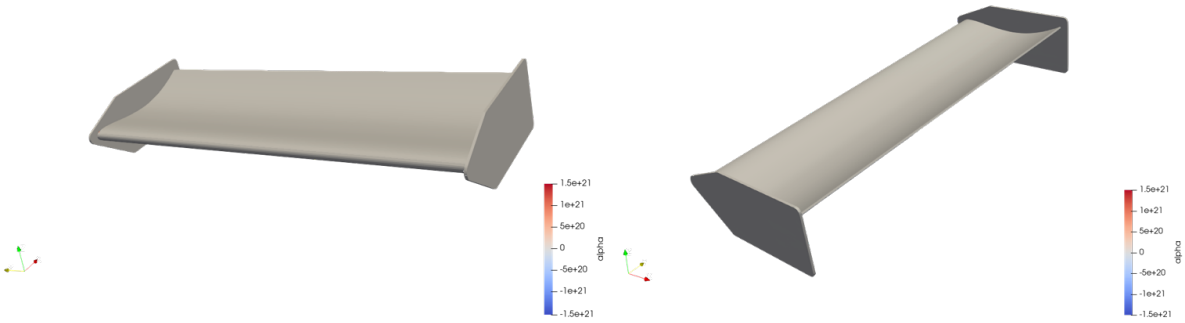

Figure 30: Sensitivity map from adjoint optimisation of Trial 3 modified rear wing

The above sensitivity map showed no areas of interest to change on the model. This implies that the gradient of the cost function is zero across the entire model, and that an equilibrium has been found. Hence, the rear wing modification from Trial 3 has achieved a local minimum of the cost function around

a neighbourhood of designs. Although this may not be a global minimum over all wing shapes, the design constraints for this problem involve seamless integration into the existing design, and regulations which prevent large changes to the wing model. This means that the viable solution is not able to take an entirely different shape than the original model, so this local minimum is a sufficient condition for optimality in this problem.

7 Triple Bottom Line

By using a CFD adjoint optimisation analysis on the rear wing the QFSAE team can increase their car's performance. The team can also apply this method to any of the part of the car's body that is designed using CAD modeling software. This includes the front wing, the cockpit, the main body of the car, etc. Doing this will improve the performance of the car and thus help the team place higher at competitions throughout the year. This success will increase their funding for multiple reasons including making it easier for the team to apply for grants such as the Shell Post-Secondary Student Development Fund and The Queen's Dean Donation Fund. It will also increase support for the team resulting in more merchandise sales. This raised interest in the team will allow them to attract more members, giving more students opportunities to gain real experience with engineering projects and build their resumes. Improving the ability of the car will also decrease it's drag and hence decrease the cars fuel consumption. Although this will be not as noticeable using just the rear wing improvements outlined in this report, using this method to improve the drag of the entire vehicle or any future vehicles the team creates will have a significant impact. Therefore, the improvements made by this optimisation will have a positive impact on the environment, by reducing emissions during their competition, will have a positive impact on the society of students in Queens engineering, by giving them more opportunities to build their engineering abilities, and it will have a positive economic impact on the team by reducing fuel cost and improving funding.

Specifically when it comes to the economic benefits of reducing fuel consumption, reducing the drag coefficient of the car by 1%, will result in a reduction of 0.444% fuel consumption [27].

Thus, even by measuring the improvements achieved using OpenFOAM analysis on an already optimised wing, the QFSAE team can expect a fuel reduction of 1.554%. Applying this to a non-optimised component of the car, when designing a whole new formula vehicle or if any part of the car is currently not optimised, the QFSAE team can expect to see significant fuel reductions which will help their budget and the environment.

8 Conclusion

By using the adjoint shape optimisation technique implemented in OpenFOAM, appropriate modifications were made to the original QFSAE rear wing design, described in Trial 3 which resulted in a drag reduction of 3.5% while maintaining 98.2% of the downforce. Even though this does not meet the design criteria of a 5% drag reduction, performing an iterative adjoint optimisation on the modified design showed local optimally of the new design. Therefore, it would not be possible to achieve any better results than this without drastically altering the design of the wing. However, these large changes break the existing criteria that the changes must be seamlessly incorporated into the existing design, and also adhere to the strict guidelines set out by the Formula SAE rules. Hence the conclusion is that the original rear wing design was near optimal, and the only improvements that can be made to the drag performance of the wing is to make the small changes to the rear profile as described in the Trial 3 modifications.

8.1 Limitations

It is important to discuss the limitation to this project and how they may have affected the accuracy of results.

8.1.1 Model Assumptions and Approximations

The first limitation arises from the inherent complexity of solving fluid dynamics equations. The model assumes that all of the approximations made when using CFD software are accurate for our application.

This includes the use of the K-ω turbulence model and the RANS quantization. It is also assumed that the mesh accurately represents the true shape. When converting a 3D object into a mesh (*.stl* file), the object is represented by triangles, approximating the true geometry. It was observed that the values for C_D and C_L vary depending on the resolution of the mesh and the software used to convert the mesh.

8.1.2 Software Tools and Hardware Capability

There are also limitations inherent to the tools used to model the system. Computational power was observed to be a highly restrictive constraint. Each simulation on the rear wing took approximately two hours to run, limiting the total number of iterations that could be modelled. Furthermore, the project team has limited experience with the SolidWorks CAD software and the OpenFOAM CFD software. This affected the actual ability to modify the 3D model in the most optimal way. This is compounded by the fact that QFSAE uses a CAD and CFD software called STAR-CCM+ which was not used in the development of this project.

8.2 Next Steps

There are still improvements to be made for this project. Specifically, the optimisation of the rear wing could be further refined with the use of different modelling tools and techniques. These options were not explored in this report due to limitations of cost and computational power.

8.2.1 STAR-CCM+

The first suggestion is to explore the use for STAR-CCM+ [28] as both a CAD software to design and modify the 3D model of the rear wing, but also as a CFD software to validate the results obtained from the OpenFOAM model. Use of STAR-CCM+ would allow for seamless integration with the QFSAE team, as they use the software for aerodynamic modelling and analysis. However, due to the cost of this software and project budget constraints, this option was not pursued.

8.2.2 Optimisation Manager in `steadyOptimisation` Mode

The next suggestion is to run the optimisation manager in the adjoint simulation to `steadyOptimisation` mode instead of `singleRun`. As mentioned in Section 4.2, in `steadyOptimisation` mode OpenFOAM will iterate through `singleRun` simulations, and automatically apply a small update to the mesh at the end of each iteration based on the sensitivity map. This was attempted on the sphere during the validation stage, however, this method requires a number of iterations in the order of hundreds or thousands. Considering that one `singleRun` simulation took approximately two hours, it is clear that pursuing this option was not viable given the project's time constraint.

8.2.3 NACA Airfoil Model

The final suggestion is to continue exploring the use of NACA 4 digit airfoils [29]. This airfoil design is defined by 4 numbers, expressed as a percentage of the wings chord length. The first two digits specify the maximum height and position of the middle camber line. The last two digits specify the thickness of the wing around it. Figure 31 shows a NACA airfoil with the camber line shown in brown, and airfoil shown in red. The max camber position is 9% up and 50% across the chord of the wing, and the thickness is at 11%. It is clear that the QFSAE team did not design their airfoil using this method, however, the NACA-9511 airfoil was found to be the NACA airfoil that most resembled the QFSAE airfoil. This was determined by minimizing the distance between points on NACA airfoils and points on the QFSAE airfoil while adjusting the four digit parameters. The NACA-9511 airfoil was then modified in SolidWorks to match the angle of attack of the QFSAE airfoil. The resulting airfoil was run through the same adjoint models as in Section 6. The coefficients of drag and lift for this wing were $C_D = 0.0333$ and $C_L = -0.288$ respectively, which is comparable to the original QFSAE wing. It is recommended that this design is iterated through using the adjoint process, making small adjustments to the 4 digits used to generate a base NACA airfoil and then adding finals detail in a CAD software like SolidWorks.

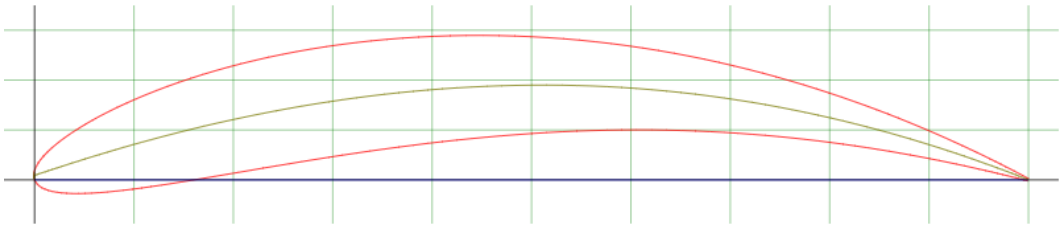

Figure 31: NACA-9511 Airfoil

References

[1] C. C. Ngo and K. Gramoll, "Fluid mechanics - theory." http://www.ecourses.ou.edu/cgi-bin/ebook.cgi?topic=fl&chap_sec=09.1&page=theory#:~:text=Note%20that%20the%20drag%20coefficient,begins%20its%20transition%20to%20turbulent. 2022-02-28.

[2] B. R. Munson, W. W. Huebsch, T. H. Okiishi, and D. F. Young, *Fundamentals of Fluid Mechanics*. John Wiley amp; Sons, Inc., 2012.

[3] G. A. A. Thuwis, R. De Breuker, M. M. Abdalla, and Z. Gürdal, "Aeroelastic tailoring using lamination parameters." https://link.springer.com/content/pdf/10.1007/s00158-009-0437-6.pdf, Oct 2009.

[4] J. Breunig, "Which turbulence model should you use for your cfd analysis?." https://www.xceed-eng.com/which-cfd-turbulence-model/, Jul 2017.

[5] M. Delaney, "Monza speed trap: who is the fastest of them all?." https://f1i.com/news/353773-monza-speed-trap-who-is-the-fastest-of-them-all.html, 2019. Accessed: 2021-10-14.

[6] P. G. Wright, "Aerodynamics for formula 1," *The Aeronautical Journal (1968)*, vol. 78, no. 761, p. 226–230, 1974.

[7] SAE International, "About - Formula SAE Michigan June." https://www.sae.org/attend/student-events/formula-sae-michigan-june/learning-objectives., 2022.

[8] J. Katz, "Aerodynamics of race cars," *Annual Review of Fluid Mechanics*, vol. 38, no. 1, pp. 27–63, 2006.

[9] SAE International, *Formula SAE Rules 2022*, August 2021.

[10] M. Cakir, "Cfd study on aerodynamic effects of a rear wing/ spoiler on a passenger vehicle." https://scholarcommons.scu.edu/cgi/viewcontent.cgi?article=1000&context=mech_mstr, 2012.

[11] T. Benson, "Navier-stokes equations." https://www.grc.nasa.gov/www/BGH/nseqs.html, May 2021.

[12] T. Benson, "Conservation of momentum." https://www.grc.nasa.gov/www/BGH/conmo.html, May 2021.

[13] C. Othmer, "Adjoint methods for car aerodynamics - journal of mathematics in industry." https://mathematicsinindustry.springeropen.com/articles/10.1186/2190-5983-4-6, Jun 2014.

[14] Nuclear Power, "Reynolds number: Definition, calculation examples." https://www.nuclear-power.com/nuclear-engineering/fluid-dynamics/reynolds-number/#:~:text=For%20external%20flow%2C%20if%20the,3500%2C%20the%20flow%20is%20turbulent., Nov 2021.

[15] C. Othmer, "Adjoint methods for car aerodynamics," *Journal of Mathematics in Industry*, vol. 4, p. 6, June 2014.

[16] M. Nayman, QFSAE Team. personal communication.

[17] C. Rumsey, "Wilcox k-omega model." https://turbmodels.larc.nasa.gov/wilcox.html.

[18] SimScale, "K-omega and k-omega sst: Global settings." https://www.simscale.com/docs/simulation-setup/global-settings/k-omega-sst/#:~:text=The%20two%20transported%20variables%20are,as%20the%20scale%20of%20turbulence., May 2021.

[19] OpenCFD Ltd., "Openfoam-v2012." https://www.openfoam.com, 2012.

[20] OpenCFD Ltd., "Simplefoam." https://openfoamwiki.net/index.php/SimpleFoam.

[21] K. Giannakoglou, E. Papoutsis-Kiachagias, and K. Gkaragkounis, *USER MANUAL; adjointOptimisationFoam, an OpenFOAM-based optimisation tool*, June 2020.

[22] BIOVIA, Dassault Systémes, "SolidWorks, 2020," 2020.

[23] "Paraview-v5.10." https://docs.paraview.org/en/latest/, 2012.

[24] L. S. Caretto, A. D. Gosman, S. V. Patankar, and D. B. Spalding, "Two calculation procedures for steady, three-dimensional flows with recirculation," in *Lecture Notes in Physics*, vol. 19, pp. 60–68, Third International Conference on Numerical Methods in Fluid Mechanics, Springer, 1972.

[25] Engineering ToolBox, "Air - density, specific weight and thermal expansion coefficient vs. temperature and pressure." [online] Available at: "https://www.engineeringtoolbox.com/air-density-specific-weight-d_600.html" [Accessed 2022-04-07], 2003.

[26] S. F. Hoerner, *Fluid-dynamic drag; practical information on aerodynamic drag and hydrodynamic resistance*. 1965.

[27] M. Rose, "Commercial vehicle fuel economy — the correlation between aerodynamic drag and fuel consumption of a typical truck," *Journal of Wind Engineering and Industrial Aerodynamics*, vol. 9, no. 1, pp. 89–100, 1981.

[28] S. D. I. Software, "Simcenter STAR-CCM+ User Guide, version 2021.1," in *Adaptive Mesh Refinement for Overset Meshes*, pp. 3067–3070, Siemens, 2021.

[29] I. H. Abbott, *Theory of wing sections : including a summary of airfoil data*. Dover Books on Aeronautical Engineering, New York: Dover Publications, 1959.

A OpenFOAM Configuration Code

```
optimisationManager singleRun;

primalSolvers
{
    op1
    {
        active                  true;
        type                    incompressible;
        solver                  simple;

        solutionControls
        {
            consistent yes;
            nIters 1000;
            residualControl
            {
                "p.*"       1.e-6;
                "U.*"       1.e-6;
            }
            averaging
            {
                average     true;
                startIter   850;
            }
        }
    }
}

adjointManagers
{
    adjManager1
    {
        primalSolver            op1;
        adjointSolvers
        {
            adjS1
            {
                // choose adjoint solver
                //-----------------------
                active                  true;
                type                    incompressible;
                solver                  adjointSimple;
                computeSensitivities    true;

                // manage objectives
                //------------------
                objectives
                {
                    type incompressible;
                    objectiveNames
                    {
                        lift
                        {
                            weight      0.25;
                            type        force;
                            patches     (RW);
                            direction   (0 0 1);
                            Aref        1;
                            rhoInf      1.225;
                            UInf        25;
                        }
                        drag
                        {
                            weight      0.75;
```

```
                            type        force;
                            patches     (RW);
                            direction   (1 0 0);
                            Aref        1;
                            rhoInf      1.225;
                            UInf        25;
                        }
                    }
                }
                // ATC treatment
                //---------------
                ATCModel
                {
                    ATCModel          standard;
                    extraConvection   0;
                    nSmooth           0;
                    zeroATCPatchTypes (wall patch);
                    maskType          pointCells;
                }
                // solution control
                //------------------
                solutionControls
                {
                    consistent yes;
                    nIters 1000;
                    residualControl
                    {
                        "pa.*"        1.e-5;
                        "Ua.*"        1.e-5;
                    }
                }
            }
        }
    }
}


optimisation
{
    sensitivities
    {
        type               surfacePoints;
        patches            (RW);
        includeSurfaceArea false;
        adjointEikonalSolver
        {
            tolerance 1.e-5;
            iters     1000;
            epsilon   0.1;
        }
    }
}
```

Listing 2: Full `optimisationDict` listing.